This manuscript was published as formal in:

CARBOHYDRATE POLYMERS Volume: 170 Pages: 60-71 Published: AUG 15 2017

https://doi.org/10.1016/j.carbpol.2017.04.055

https://www.sciencedirect.com/science/article/pii/S014486171730454X

Title:

Development of Biocompatible Glycodynameric Hydrogels Joining two Natural Motifs by Dynamic Constitutional Chemistry

by:

Luminita Marin[1*], Daniela Ailincai[1], Simona Morariu[1], Liliana Tartau-Mititelu[2]

[1] "Petru Poni" Institute of Macromolecular Chemistry of Romanian Academy, Iasi, Romania

[2] "Gr .T. Popa" University of Medicine and Pharmacy University, Iasi, Romania

*Corresponding Author Luminita Marin

e-mail: lmarin@icmpp.ro

ABSTRACT

The paper focusses on the synthesis of novel hydrogels by joining natural biodegradable compounds with the aim to achieve biocompatible materials for bio related applications. The hydrogels were prepared from chitosan and citral by constitutional dynamic chemistry, incorporating both molecular and supramolecular dynamic features. The hydrophobic flexible citral has been reversible immobilized onto the hydrophilic chitosan backbone *via* imine bonds to form amphiphilic glycodynamers, which further self-ordered through supramolecular interactions into a 3D-network of biodynameric hydrogel. The synthetic pathway has been demonstrated by NMR and FTIR spectroscopy, X-ray diffraction and polarized light microscopy. Studies of the hydrogel morphology revealed a 3D porous microstructure, whose pores size correlated with the crosslinking degree. Rheological investigations evidenced high elasticity, thermo-responsiveness and thixotropic behavior. As a proof of the concept, the hydrogels proved *in vivo* biocompatibility on laboratory mice. The paper successfully implements the constitutional dynamic chemistry in generation of chitosan high performance hydrogels.

KEYWORDS: hydrogel, chitosan, dynamic constitutional chemistry, rheology, biocompatibility

1. INTRODUCTION

Hydrogels are a class of soft materials mainly composed of water, with modulable structure and functions and so with a plenty of applications in important fields of the human life – as substrates for biomedical engineering and pharmacology, environmental protection, agriculture, food industry, hygiene and so on [Chawla, Srivastava, Pandey, & Chawla, 2014; Chen et al. 2016; Jayakumar et al., 2010; Jing, Wang, Yu, Amer, & Zhang, 2013; Kamata, Li, Chung, & Sakai, 2015; Sharma et al., 2014]. Among hydrogels, those prepared from natural polymers present the advantage of bioactivity, biocompatibility and biodegradability, being especially studied for bio-related applications. In particular, chitosan-based hydrogels have the highest *in vivo* applicability due to the intrinsic properties of chitosan, such as biocompatibility and biodegradability, hemostatic, hypolipidemic, hypoglycemic, antitumoral, antimicrobial and fungicidal activity – to mention only some [Jayakumar, Menon, Manzoor, Nair, & Tamura, 2010; Padmanabhan, & Nair, 2016]. The traditional pathways of chitosan gelling use either physical crosslinkers leading to hydrogels with weak mechanical properties and uncontrolled dissolution, or chemical crosslinkers resulting in hydrogels with better mechanical strength and the advantage of controllable morphology [Padmanabhan, & Nair,

2016]. Since chitosan is in fact a polyamine, the main route of its chemical crosslinking is the acid condensation reaction between its amine functional moieties and dialdehydes giving imine bonds. The most encountered crosslinking agent is glutaraldehyde, which was recently demonstrated to have a certain degree of toxicity for the human body [Beauchamp, St Clair, Fennell, Clarke, & Morgan, 1992; Berger et al., 2004], fact which turned the attention of the scientific community to more friendly crosslinkers originating from natural sources, especially targeted due to their potential to preserve the biological properties and to mimic the natural tissues [Beskardes, Demirtas, Durukan, & Gumusderelioglu, 2015; Garnicia-Palafox, & Sanchez-Arevalo, 2016; Huber et al., 2017; Mikhailov et al., 2016]. Even if so much effort has been dedicated to the obtaining of chitosan based hydrogels, less attention has been paid to the potential of the imine bonds formed on the chitosan chains. Imine bonds, also known as azomethines or Schiff bases, were extensively studied for their high thermostability, thermotropic properties, ability to act as ligand, semiconducting and luminescent properties [Kaya, & Kilavuz, 2015; Sek et al., 2012; Zabulica et al. 2013; Zabulica, Perju, Bruma, & Marin, 2014; Zaltariov et al., 2015]. In addition to the above mentioned properties, lately, the reversibility of the imine bonds proved to be the most important tool in (i) dynamic covalent chemistry conferring advantageous proof reading and error checking capabilities toward supramolecular entities [Chen et al., 2013; Chen et al., 2013; Liu, & Li, 2013; Liu, Lehn & Hirsh, 2016; Roy, Bruchmannb, & Lehn, 2015; Schneider, Siegfried Hauswald, Stoll, & Mastalerz, 2012] and (ii) dynamic combinatorial chemistry toward constitutional libraries whose constituents can exchange under the pressure of external factors generating adaptive chemical systems [Clima, Peptanariu, Pinteala, Salic, & Barboiu, 2015; Hu, Zhang, & Ramström, 2015; Marin et al. 2016; Sreenivasachary, & Lehn, 2005; Zhang, & Barboiu, 2016]. By dynamic covalent chemistry, challenging supramolecular architectures have been created, such as epitaxial crystals [Chen et al. 2013], microtubes [Chen et al., 2013], molecular cages, porous organic amorphous or crystalline materials [Schneider, Siegfried Hauswald, Stoll, & Mastalerz, 2012], self-healing films [Roy, Bruchmannb, & Lehn, 2015] and hydrogels [Chang, Wang, Li, An, & Qin, 2016]. Moreover, it was demonstrated that the imine linkage has the potential to drive a gelation process selecting an organogelator from a library, and plays a key role in gelling process due to its conjugation which favors the assembly of the gelator network [Sreenivasachary, & Lehn, 2005].

Recent and challenging studies in the area of hydrogels revealed that the obtaining of hydrogels using multi-valence binders led to superior mechanical strength and substantial elastic response of such systems which are mostly composed of water [Wang et al., 2010].

Outstanding, controllable mechanical properties were reached also for hydrogels with layered morphology induced by the use of metallic nanosheets [Liu et al., 2013].

Here we present a new approach for the preparation of hydrogels using the citral monoaldehyde as chitosan gelator, based on dynamic imine chemistry. Citral is a natural, relatively long chain, aliphatic monoaldehyde found in the oil of several plants, with lack of toxicity to the human body (LD_{50} values more than 1000 mg/Kg), rapidly metabolized and excreted as metabolites [SIDS, 2001], increasing the potential of its use in preparation of new biocompatible and biodegradable materials. Detailed characterization studies demonstrated that the unusual gelation of chitosan in the presence of citral was driven by the competition between the imine formation and its aliphatic side chains self-organization into supramolecular layered architectures. Thus, ordered entities were obtained which in turn played the role of multi-binder crosslinkers of chitosan chains giving raise to hydrogels with remarkable mechanical properties.

2. EXPERIMENTAL SECTION

2.1. Materials

Citral (95%), low molecular weight chitosan (263 kDa, DA: 83%), D-glucosamine hydrochloride and phosphate buffer solution have been purchased from Aldrich and used as received. Acetate buffer (pH=4) was prepared in our laboratory [Iftime, Morariu, & Marin, 2017].

2.2. Synthesis of the model compound

The model compound has been synthesised according to a published procedure [Safoura et al., 2014], slightly modified taking into consideration the properties of citral, as follows: 100 mg D-glucosamine hydrochloride (0.463 mmol) have been solubilized in 1.4 mL methanol and mixed under vigorous stirring with a stoichiometric amount of sodium hydroxide (0.018 g; 0.463 mmol), with the purpose to obtain the free amine. After five minutes, the mixture has been filtered to remove the resulted salt. To the clear solution of the free glucosamine, 0.074 g (0.463 mmol) of citral have been added, at 35 ^{o}C, and kept under magnetically stirring about five minutes, when a white precipitate formed. The precipitate was filtered, washed three times with cold dichloromethane and dried under vacuum for 24 hours.

^{1}H NMR (DMSO-d_6, 400 MHz) δ(ppm): 8.07, 8.05, 8.04, 8.02 (d, 1H, H_h); 6.45 (s, 1H, OH from sugar unit), 5.88, 5.86 (d, 1H, OH from sugar unit), 5.1 (m, 1H, H_c), 4.99 (s, 1H, OH from sugar unit), 4.78 (m, 1H, OH from sugar unit), 4.58 (m, 2H, H_o), 3.71 (d, 1H, H_g), 3.17,

3.15 (superposed peaks, 2H, H_k, H_j); 3.48 (superposed peaks, 1H, H_n); 2.64, 2.31 (m, 2H, H_e); 2.13 (superposed peaks, 3H, H_f); 1.9, 1.85 (s, 2H, Hd); 1.66 (s, 3H, Hb); 1.59 (s, 3H, Ha). FT-IR (ATR, cm^{-1}): 3424 (ν_{OH}); 2904, 2839 ($\nu_{CH2,}$ ν_{OH}); 1644 ($\nu_{CH=N}$); 1618 ($\nu_{C=C}$); 1441, 1381 (ν_{C-H}); 1083 ($\nu_{C-O-C\ pyranose}$); 897 (δ_{C-H}).

2.3. Preparation of hydrogels and xerogels

Firstly, solutions of the two reagents were prepared by dissolving chitosan (0.06 g, 0.29 mmoles of glucosamine repeating units) in 0.7% acetic acid aqueous solution (3 mL) to give a 2% solution, and by dissolving different amounts of citral in alcohol to give a 1% solution (Table 1). The amount of chitosan has been kept constant while the amount of aldehyde was varied, in order to obtain hydrogels with different crosslinking degrees labelled as in Table 1. Then, the citral solution has been added drop wise to the chitosan one, under continuous magnetic stirring at 55 ^oC up to the visual examination revealed the transformation of the pallor solution into a transparent yellowish semisolid, without air bubbles or other macroscopic particles. In the case of the sample **C1** the gelation occurred immediately after the entire amount of citral was added, while in the case of **C2**, a semisolid hydrogel was obtained after 3 hours. For the other samples, hydrogels were obtained only after 24 hours. The sample **C4.5** remained as a highly viscous liquid even after 24 hours. All hydrogels were kept uncovered until they reached the same level as the initial solution of chitosan, indicating the removal of ethanol. The hydrogels were kept covered another ten days to reach the equilibrium of the imination reaction (according to the NMR experiments), and then sent to experimental characterization. Corresponding xerogels were obtained by lyophilisation. By weighing the precursor reagents and the xerogels it was found that no reagents were removed during lyophilization (Table 1).

Table 1. The codes and the corresponding NH_2/CHO molar ratio of the hydrogels

Code	**C0**	**C1**	**C2**	**C2.5**	**C3**	**C3.5**	**C4**	**C4.5**
NH_2:CHO ratio	1:0	1:1	2:1	2.5:1	3:1	3.5:1	4:1	4.5:1
mg/mmol of chitosan	60/0.29	60/0.29	60/0.29	60/0.29	60/0.29	60/0.29	60/0.29	60/0.29
mg/mmol of citral	0	46/0.29	23/0.145	18/0.116	15/0.096	13/0.082	11.6/0.0725	10/0.064
mg of xerogel	60	106	83	78	75	73	71.6	70
Gelation time	-	3 min	3 hours	24 hours	24 hours	24 hours	24 hours	-

2.4. Methods

Nuclear magnetic resonance (NMR) spectra of the model compound and hydrogels were recorded in deuterium oxide using a Bruker Avance DRX 400 MHz Spectrometer equipped with a 5 mm QNP direct detection probe and z-gradients. The chemical shifts are reported as

δ values (ppm) relative to the residual peak of the solvent. NMR spectra were registered at each three days to establish the stabilization of the imination equilibrium. All–spectra have been processed using TopSpin 1.3 software.

Fourier transformed infrared (FTIR) spectra of the model compound, chitosan and xerogels were measured with a FT-IR Bruker Vertex 70 Spectrofotometer, by ATR technique. All spectra have been processed using OPUS 6.5 software.

Wide angle X-ray diffraction (WXRD) has been done on xerogel pellets, using a Bruker D8 Avance diffractometer with the Ni-filtered Cu-Kα radiation (λ = 0.1541 nm). The data were recorded at 36 kV and 30 mA and the results have been handled using FullProf 2000 software. The diffractograms have been registered between 2-40° (2 theta degrees). The xerogels pellets were obtained by pressing with a manual Hydraulic Press, at 10 N/m^2.

Polarized light microscopy observations were performed on thin slices of hydrogel between two clean untreated glass slides, using an Olympus BH-2 polarized light microscope.

The microstructure of the hydrogels has been characterized by surface and cross-section viewing with a field emission Scanning Electron Microscope SEM EDAX – Quanta 200, operated at 12.5 or 20 keV accelerating voltage. The images have been handled using Image J Software in order to determine the pore size and the thickness of the pore walls. Resulted data were used to build the histograms and to determine the standard deviation values in Origin Software.

The gelation time has been determined as the period of time after which the reaction mixture has been visually transformed from a viscous liquid into an elastic quasi solid state.

The swelling measurements have been performed on square-shape pieces of xerogels which were kept in the oven over night. The measurements were performed in triplicate, using always the same amount of water or buffer solution (20 mL). By weighing the mass of the samples before and after swelling, the mass equilibrium swelling (MES) has been calculated using the equation: MES = (Ms-Md)/Md, where Ms is the mass of the hydrogel in swollen state and Md the mass of the hydrogel in dried state.

The rheological parameters were determined using a Bohlin CVO rheometer with parallel plate geometry (60 mm diameter) and thermal control by the Peltier effect in closed system. The frequency sweep experiments were carried out at 20 °C and 37 °C, respectively, within the linear viscoelastic regime. The amplitude sweep tests have shown an extended linear viscoelastic domain corresponding to structured samples [Morariu, Bercea, & Brunchi, 2015]. The oscillatory and continuous shear measurements were performed in the frequencies

range of 0.5 – 100 rad·s^{-1} and in the range of shear rate ($\dot{\gamma}$) from 6 x 10^{-2} s^{-1} to 10^{2} s^{-1}. From the oscillatory deformation tests, the loss modulus (*G''*), the storage modulus (*G'*), the complex viscosity (η^*) and the loss tangent ($tan\ \delta$) defined as *G''*/*G'* were determined. In addition, the flow tests were performed at 20 °C in order to obtain the hysteresis loops by increasing the shear rate up to 400 s^{-1} in 500 s followed by its reduction from 400 s^{-1} to 0 in the next 500 s. For **C1** sample, at 20 °C, some rheological measurements were not possible due to its brittleness.

The hydrogels were frozen in liquid nitrogen and further submitted to lyophilization using a Christ Alpha 2-4 LD plus, Freeze Dry equipment, for 24 hours at -50 ºC and 0.04 mbar.

In vivo biocompatibility of the hydrogels. The *in vivo* biocompatibility of the hydrogels was evaluated by determining the hematological, biochemical and immune system profile of animals treated with the tested substances (saline solution, **C1**, **C2**, **C3**). For these investigations were used Swiss white mice (weighing between 25-30g) with uniform distribution by gender, purchased from the bio-base of ''Grigore T. Popa'' University of Medicine and Pharmacy, Iaşi. The animals were brought one day before, and kept in standard laboratory conditions (with 21°C±2°C constant temperature, 50-70% relative humidity and an alternating lighting regime, with ratio of light/darkness = 12 hours/12 hours), with food and water available *ad libitum*. Before the experiment, mice were placed upon a wire mesh, in a plastic box and left for two hours to acclimatize to the laboratory environment. In order to avoid the chrono-biological influences, the tests were carried out in the interval between 8-12 a.m. For biocompatibility estimation, 4 groups of 6 animals each were treated intraperitoneally (i.p.) as follows: **Group 1** (coded **Control**): saline solution 0,1 mL/10g body weight - control; **Group 2** (coded **C1**): hydrogel **C1**; **Group 3** (coded **C2**): hydrogel **C2**; **Group 4** (coded **C3**): hydrogel **C3**. After 24 hours and 14 days from the intraperitoneally administration of investigated substances, the animals were anaesthetized with ethyl ether and the blood was collected from the retro orbital plexus to asses (i) the hematologic profile: - the values of erythrocytes (ER), hemoglobin (Hb), hematocrit (Ht); - the white blood cell differential: polymorphonuclear neutrophils (PMN), lymphocytes (Ly), eosinophils (E), monocytes (M), basophils (B); (ii) the liver enzymes activity: - the alanine aminotransferase, also called the glutamate pyruvate transaminase (GPT); - the aspartate aminotransferase, also called glutamic oxaloacetic transaminase (GOT); - the lactic dehydrogenase (LDH); (iii) the levels of some immune system parameters: - the phagocytic capacity of neutrophils in the

peripheral blood (PC); - the serum opsonic capacity (OC); - the phagocytic and bactericidal capacity of peritoneal macrophages (BC).

For biochemical analysis, 0.3 ml of venous blood has been drawn from the retro orbital plexus after topical anesthesia. Blood samples were collected in heparinized tubes and kept in an ice-water mixture until the moment of determination. Laboratory tests were performed using the special Analyzers for each investigated parameters [De Jong, Carraway, & Geertsma, 2012; Limon-Pacheco, & Gonsebatt, 2009; Wolf, & Andwraon, 2012].

On the 14^{th} day of the experiment the serum opsonic capacity (OC) was evaluated by using the cultures of *Staphylococcus aureus 94*.

At the end of the experiment, the animals were euthanized under ethyl ether anesthesia and the peritoneal macrophages were removed from the intact peritoneal cavity with 10 ml HANKS solution (thermostatated at 37^0C). The samples were centrifugated at 1000 rpm for 10 minutes, brought into contact with *Staphylococcus aureus 94* cultures, incubated for 48 hours at 37^oC and re-inseminated on culture media. The following immune parameters activity: phagocytic capacity (PC) and bactericidal capacity (BC) of peritoneal macrophages was investigated.

All the data were centralized and statistically analyzed using Student's t-Test in EXCEL program for Windows 10. Results were expressed as mean values ± standard deviation of the mean for 6 animals in a group. The p values less than 0.05 were considered to be statistically significant comparative to those of the control group.

The liver fragments were collected for histopathological examination. Tissue fragments were fixed in 10% formalin, embedded in paraffin and hematoxylin&eosin (H&E) stained. The samples were examined and visualized using an optical microscope equipped with a digital system for images acquisition.

The experiments were performed according to the recommendations of the "Grigore T. Popa" University Committee for Research and Ethical Issues in compliance with the international regulations regarding the handling of the laboratory animals. Particularly, the duration of the experiments was the shortest possible and the number of animals used in has been reduced to the minimum sufficient to achieve adequate statistical processing of the obtained data. For ethical reasons all animals used in study have been sacrificed at the end of the experiments.[11]

3. RESULTS AND DISCUSSIONS

A series of hydrogels has been obtained by reacting chitosan with citral in various molar ratios of the functional groups. The obtained hydrogels were transparent, yellowish under normal light and emitted blue light by illumination with an UV lamp (Scheme 1). The hydrogels will be referred to by the letter **C** followed by the number representing the molar ratio between the amine groups on chitosan and aldehyde functionality of citral, e.g. the hydrogel with a NH_2/CHO molar ratio of 2/1 was noted **C2**.

The crosslinking of chitosan with citral mono-aldehyde is an unprecedented pathway of hydrogel preparation which requires a detailed structural characterization in order to understand the driving forces governing the gelling process. To reach this goal a model compound (**MC**) was synthesized from glucosamine (the repeating unit of chitosan) and citral and analyzed as a reference. The main chemical reaction most likely to take place between the polyamine-like chitosan and citral is the acid condensation of the amino group and the electrophile carbonyl to give the imine linkage. On the other hand, it must be considered that the formation of imine in water is a reversible reaction which allows imination and trans-imination processes under the pressure of external stimuli giving a dynamic material [Chen et al., 2013; Chen et al., 2013; Liu, & Li, 2013; Roy, Bruchmannb, & Lehn, 2015; Schneider, Siegfried Hauswald, Stoll, & Mastalerz, 2012]. To monitor the chemical and physical transformations during the chitosan gelling process in the presence of citral, ^{1}H-NMR and FTIR spectroscopies were involved.

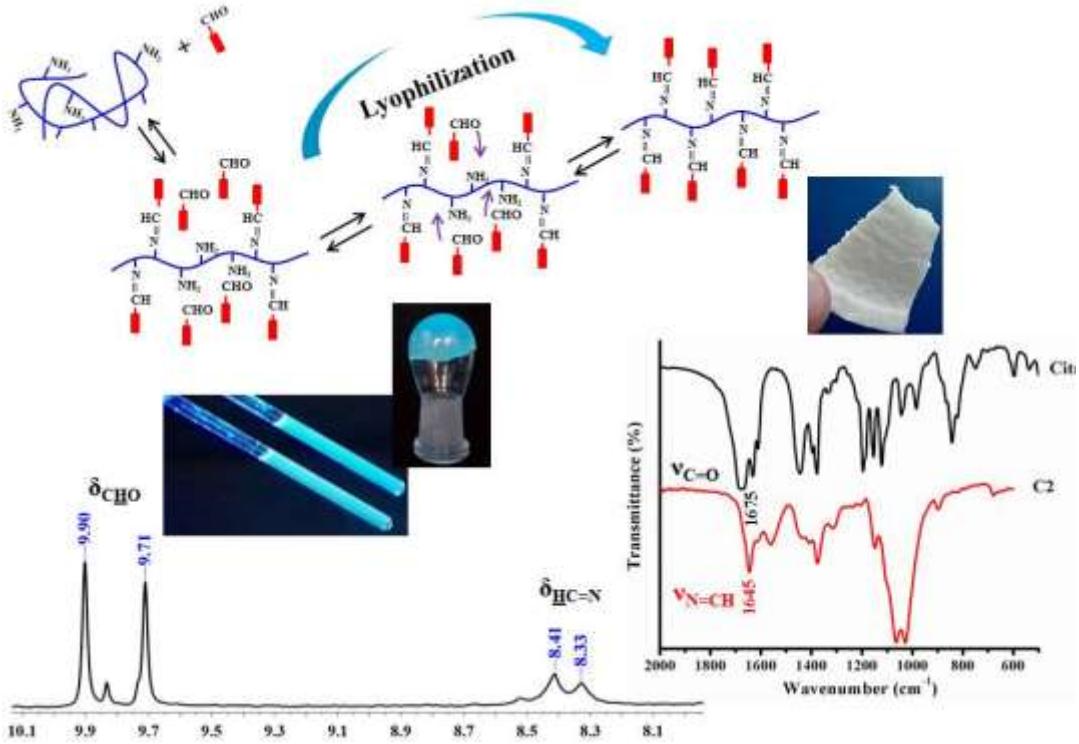

Scheme 1. Representation of the synthesis of the hydrogels and corresponding xerogels, highlighting the imine formation by ^{1}H-NMR and FTIR spectra

3.1. NMR characterization

^{1}H-NMR evidenced the formation of the imine linkage by the presence of the specific chemical shift of the imine proton between 8 and 9 ppm [Marin, van der Lee, Shova, Arvinte, & Barboiu, 2015; Safoura, 2014]. The chemical shift of the imine proton in the model compound appeared as a pair of doublets located at 8.07, 8.05 and 8.04, 8.02 ppm, due to the *cis* and *trans* conformers (Figure S1) [Ailincai et al., 2016; Destri, Khotina, & Porzio, 1998]. The hydrogel spectra showed the chemical shift characteristic to the imine proton but also that of the aldehyde proton indicating an equilibrium reaction (Scheme 1, Figure S2a). The signal of the imine proton was shifted to a higher magnetic field at 8.41, 8.32 ppm, corresponding to a deshielding effect consistent with a stronger conjugation of the newly formed imine units in hydrogels, probably, gained due to the H-bonding and self-organization of the imine units [vu Deb Linde, Dornseiffen, Veenland, & de Boer, 2016]. The monitoring of the evolution of the NMR spectra over time revealed that the equilibrium position of the imine formation reaction slowly shifted toward imine products during 10 days (Figure S2b), reaching a 1/1 molar ratio of the newly formed imine to unreacted aldehyde (Figure S2c). This suggested the sol-gel transition as a stimulus which favored the imine formation by imination and transimination

reactions, specific to the dynamic systems [Chen et al., 2013; Liu, & Li, 2013; Marin et al., 2014; Roy, Bruchmannb, & Lehn, 2015; Schneider, Siegfried Hauswald, Stoll, & Mastalerz, 2012].

3.2. FTIR characterization

To put into evidence the chemical pathway of the hydrogel formation, FTIR spectra of the model compound and chitosan-citral xerogels were recorded. In the **MC** spectrum, the characteristic stretching vibration band of the imine group clearly appeared as a sharp peak at 1645 cm^{-1} in the fingerprint region, while the bands characteristic to the aldehyde (1675 cm^{-1}) and amine (1560 cm^{-1}) groups of the reagents were missing (Figure S3). Compared to the aromatic imines, the -CH=N- band is shifted to higher wavenumbers, in agreement with the lower degree of conjugation of the imine bonding two aliphatic units [Marin, Simionescu, & Barboiu, 2012; Sek, Grucela-Zajac, Krompiec, Janeczek, & Schab-Balcerzak, 2012]. As can be seen in figure 1a, the imine band in the FTIR spectra of the **C** xerogels is similar in terms of position and shape, except a left tail of low intensity which belongs to the aldehyde group, indicating traces of unreacted citral. The intensity of the imine band increased as the citral content in hydrogels increased, corresponding to a higher density of the imine linkages. Simultaneously with the appearance of the imine band, the deformation vibration band of the N-H linkage (1556 cm^{-1}) of the amine units of chitosan drastically diminished in intensity indicating its consuming. Comparing NMR and FTIR data (Scheme 1) it can be concluded that the imination reaction further proceeded during the lyophilization process, due to the slowly removal of water which shifted the reaction equilibrium to the products [Marin et al., 2014; Marin et al., 2015]. This was possible because of the water H-bonded, residual ethanol and acetic acid which ensured an appropriate environment for the condensation reaction [Dinu, Ozmen, Dragan, & Okay, 2007].

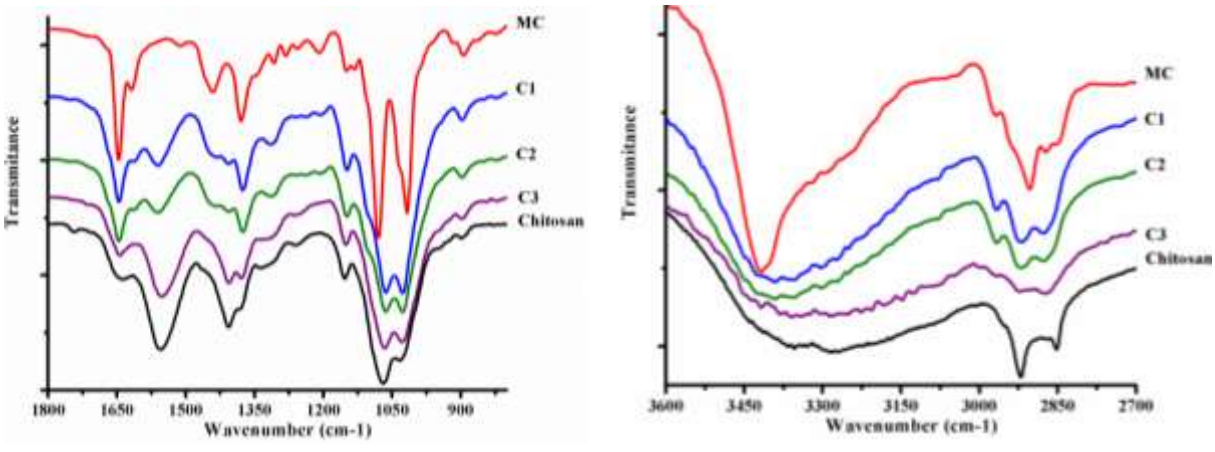

Figure 1. FTIR spectra of the chitosan, model compound and some representative xerogels

The morphology of the solid state of chitosan is dominated by the H-bonds, intra- and intermolecular ones, reflected in the FTIR spectra in the 2700 – 3700 cm^{-1} and 1200 – 1500 cm^{-1} domains [Kumirska et al., 2006; Marin et al., 2014]. Thus, in the chitosan spectra appeared two overlapped bands at 3375 cm^{-1} and at 3275 cm^{-1} corresponding to the stretching vibrations of the hydroxyl groups involved in intramolecular and intermolecular H-bonds, respectively (Figure 1b). In the spectrum of the **MC**, the band corresponding to the intermolecular H–bonds appeared only as a shoulder, while the band corresponding to the intramolecular H-bonds was intense, slightly shifted to higher wavenumbers indicating their prevalence. Looking to the **MC** structure, the formation of an intramolecular H-bond is favored between the proton of the imine linkage and an oxygen atom of a hydroxyl group of glucosamine in a neighbor position, giving a more stable six-membered cycle compared to a five-membered cycle which should be formed by an intramolecular H-bond between the imine nitrogen and a hydrogen atom of a hydroxyl group of glucosamine. The **C** xerogel spectra present high similarity in this spectral region with that of the model compound. The band at 3375 cm^{-1} was more shifted to higher wavenumbers as the amount of citral into xerogels increased, consequence of a close correlation between the formation of the imine linkages and intramolecular H-bonding. Compared to the model compound, the band at 3275 cm^{-1} was still quite intense, indicating the presence of the intermolecular H-bonds, too.

Another significant change in the spectra of the MC and xerogels compared to that of chitosan was revealed in the absorption band characteristic to the CH_2 bending, whose shape and intensity are strongly correlated to the hydrogen bonds environment. In this region chitosan exhibited an overlapped band with the intensity maximum at 1405 cm^{-1} and a shoulder at 1377 cm^{-1} which underwent significant changes in the case of the xerogel samples, namely increasing the absorption intensity at 1377 cm^{-1}, while decreasing the peak at 1405 cm^{-1} to a shoulder (Figure 1a). This pronounced intensity exchange of the two overlapped bands indicates considerable alteration of the H-bonds environment given by a drastic modification of morphology.

3.3. Supramolecular characterization

The X-ray diffraction method was involved in order to understand better the influence of grafting side chain imine units on chitosan on the morphology and therefore on the gelling process. Chitosan was demonstrated to have a semicrystalline morphology consisting of ordered clusters of dried chitosan, dispersed into the amorphous state of hydrated chitosan [Leceta, Guerrero, Ibarburu, Dueñas, & de la Caba, 2013], as evidenced by two broad overlapped bands with the reflection maxima around 12 and 21 ^{o} (Figure 2a).

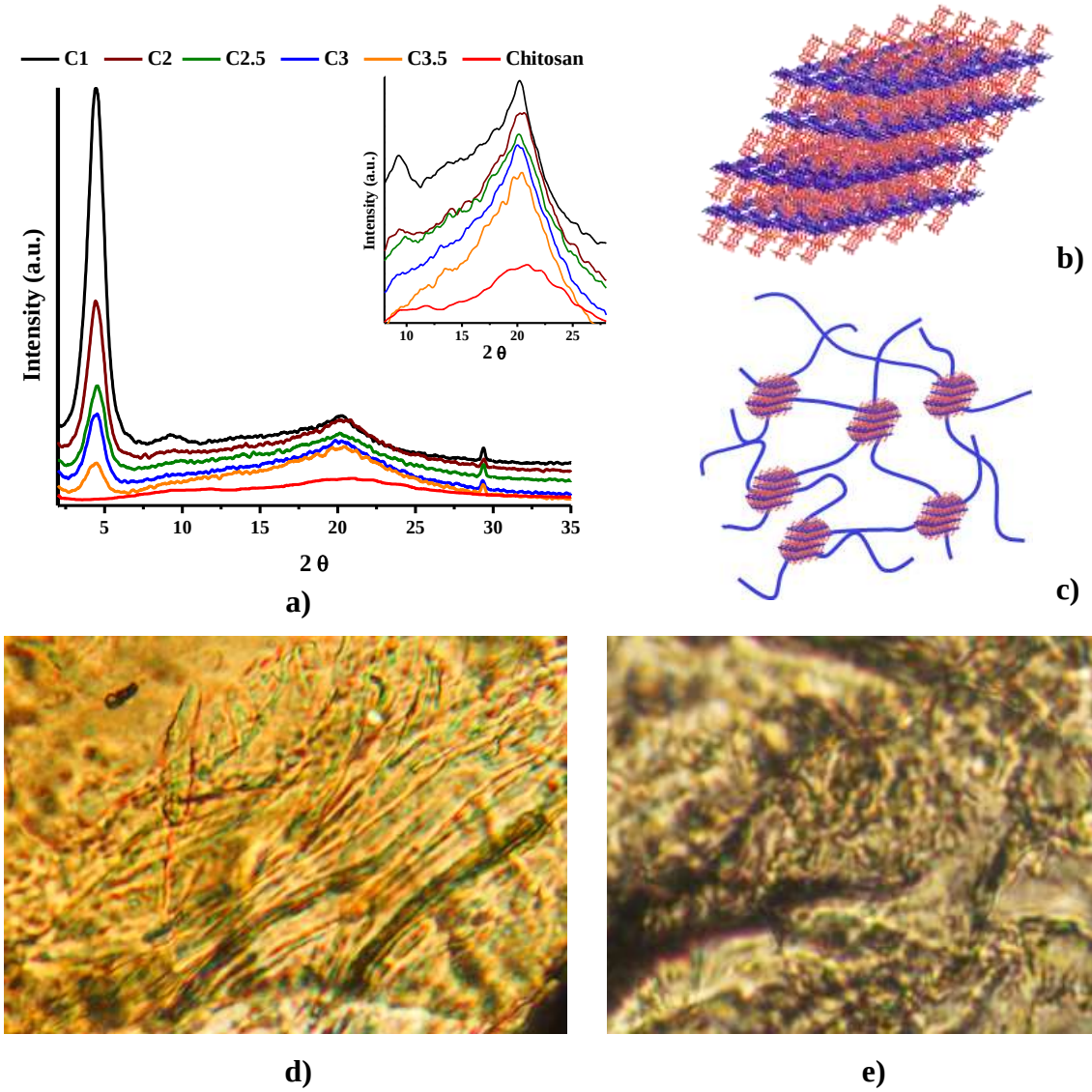

Figure 2. a) WXRD curves of chitosan and some representative hydrogels; b) Representation of the layered architecture; c) Representation of the hydrogel network for non-stoechiometric ratios of the functional groups; d), e) Representative POM microphotographs of **C1** showing streaky textures, magnification 200x

Compared to the chitosan X-ray diffractogram, the **C** xerogels have a completely different pattern, confirming the drastic morphological changes by imine grafting (Figure 2a). Firstly, it was characterized by a very intense reflection band in the small angle domain (4.3 – 4.7 º) corresponding to a d-spacing of 20.55 – 18.80 Å, defining a layered periodicity. The reflection was more intense as the imine linkage density increased, attributed to longer-range ordering [Suryanaraya, & Grant, 1998]. In the wide angle domain, the broad reflection band at 20.4º, caused by the intramolecular distances in chitosan [Leceta, Guerrero, Ibarburu, Dueñas, & de la Caba, 2013], was still present, but sharper and of higher intensity attributed to the

increasing of the persistence length of the chitosan chains favored by the grafting of the imine units. The reflection band in the middle angle domain was also sharper and more intense for xerogels compared to the chitosan, especially in the case of **C1** (characterized by the highest density of the imine units), attributed to the intermolecular correlations among the imine units [Ailincai et al., 2016]. As a whole, the X-ray pattern of the studied xerogels is reminiscent of that of smectic A mesophase of the thermotropic liquid crystals, characterized by a well-defined periodicity of molecules layers in which the mesogens tend to lay with the long axes perpendicular to the layer planes and have no long-range positional order of their centers of mass [Baron, 2001; Dabrowski, 2015; Marin, Destri, Porzio, & Bertini, 2009]. The explanation of this unusual layering of chitosan obtained by grafting side chain aliphatic units on its semiflexible backbones can be found if we take in consideration the self-ordering ability of the imine units stabilized by intramolecular H bonds and the antagonistic nature of the hydrophilic chitosan and hydrophobic side chain aliphatic imine grafted on it, which guided the segregation of hydrophilic/hydrophobic layers (Figure 2b). Combining the data of the three methods of structural characterization (FTIR and NMR spectroscopy and X-ray diffraction) the scenario of the gelling process can be drawn as follow.

At 55 ^{o}C, chitosan in solution undergoes the complete destabilization of the intra-chain H- bonds when the persistence length decreased rapidly and the local stiffness was lost, chitosan being characterized by a coiled conformation [Rinaudo, 2006]. By adding the citral solution, the condensation reaction between amino groups of chitosan and aldehyde units of citral took place *via* imine rigid linkage yielding amphiphilic macromolecules whose antagonistic building blocks segregated in layers favored by the imine tendency to self-organize, similar to lyotropic liquid crystals with lamellar mesophases (Figure 2b) [Amar-Iuli, & Garti, 2006]. Due to the high degree of reversibility of the imine formation in aqueous medium, the reaction equilibrium between reagents and imine units was reached. Most probably, the unreacted aldehyde aggregates with the side chain aliphatic tail of the newly formed imine units grafted on chitosan backbone chain, thus leading to hydrophobic associations bearing a hierarchical structure with parallel stacked layers (Figure 2b). The hydrophilic chitosan layers were consolidated by the H-bond system, while those of aliphatic side chains by hydrophobic interactions, demonstrated as being stronger in the case of hydrocarbon chains than the aromatic ones [Desbrires, Martinez, & Rinaudo, 1996]. Thus, the chitosan gelling proceeded once the ordering process took place, being in fact the result of the competition of three dynamic processes: (i) reversible covalent imine formation (ii) imine aliphatic side chains self-organization in hydrophobic associations and (iii) segregation of

hydrophobic/hydrophilic layers. The formation of the hydrophobic layers increased the accessibility of the unreacted aldehyde to the amine sites and thus favored its conversion into the imine units by imination and transimination processes which took place under the pressure of the self-ordering into a hierarchical system of higher stability, specific to the dynamic imine chemistry [Liu, & Li, 2013]. Moreover, the minimal contact with water of the hydrophobic layers during the lyophilization process further facilitated the shift of the reaction equilibrium to the imine products. Taking into account, that (i) no citral loss take place during lyophilization; (ii) only small traces of citral were evidenced by FTIR; (iii) a close relationship between the magnitude of long-range layer order and the imine density was revealed by WXRD, it can be considered that a lamellar structure was reached in the case of **C1** (Figure 2b), and ordered lamellar entities acting as multibinder net nodes of chitosan free chains in the case of the other hydrogels (Figure 2c). As the reaction took place in non-equimolar conditions, the size and density of the lamellar entities varied with the imine linkage density. The formation of the supramolecular net nodes has been also suggested by TEM measurements, when black spots could be distinguished (Figure S4).

A supramolecular arrangement has to show a distinct texture when viewed through a cross-polarized microscope [Baron, 2001; Dabrowski, 2015; Marin, Destri, Porzio, & Bertini, 2009]. As can be seen in figure 2d,e, the hydrogels exhibited “streaky” birefringent textures under polarized light, typical to lamellar mesophases of the lyotropic liquid crystals, once more confirming the supramolecular architecture of the hydrogels.

3.4. Hydrogel microstructure

The xerogels showed a sponge-like microstructure with pore diameter varying with the content of aldehyde crosslinker in each hydrogel; the pore diameter increased from 14 to 26 μm as the content of citral decreased (Figure 3). The hydrogels with smaller amount of citral and so lower density of lamellar entities and higher density of hydrophilic chitosan showed larger pores. Compared to other chitosan hydrogels [Marin et al., 2014], they had smaller inner pore size, attributed to the hydrophobic citral layers which limited the water entrapping during the gelling process.

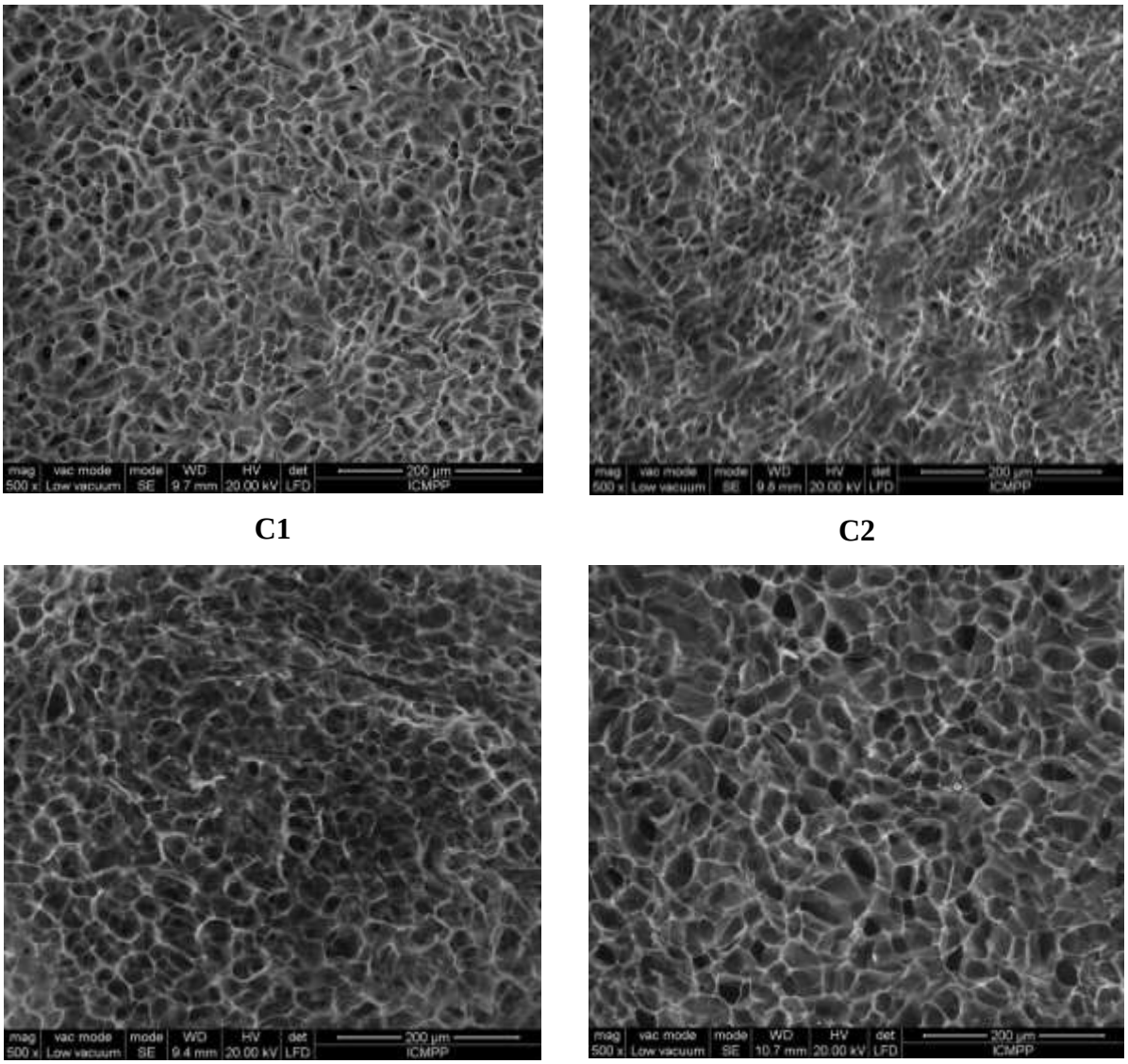

Figure 3. SEM microphotographs of the hydrogels

3.5. Rheological properties

Rheological investigations of the studied hydrogels were performed in order to gain information related to their mechanical strength correlated to their crosslinking degree and subsequent to their supramolecular architecture. In frequency sweep experiments, carried out at 20 °C in the linear domain of viscoelasticity, the samples showed the dominance of the elastic component over the viscous one (*G' > G"*, solid-like behavior) for molar ratios of NH_2/CHO below 3.5 (**C1-C3.5**). The values of the elastic modulus are high at high frequencies, comparable with those of hydrogels obtained using multi-branched crosslinkers [Wang et al., 2010], indicating robust mechanical properties. Particularly, the value of the elastic modulus of the **C1** hydrogel with layered morphology is significant higher compared

to the other hydrogels cross-linked by supramolecular entities (from 5 to 72 times, as the crosslinking degree decreased) (Table S1). As the NH_2/CHO molar ratio increased, the viscous component became slightly dominant over the elastic one ($G' < G''$) in the case of the **C4.5** sample, indicating a liquid-like behavior near the gel point (Figure 4a). Considering the power law dependence of the viscoelastic moduli on frequency, $G'(\omega) \sim \omega^{n'}$ and $G''(\omega) \sim \omega^{n''}$, the gel point was determined, according to Chambon and Winter [Chambon, & Winter, 1987], which established that at the gel point, $n' = n'' = n$, and the following scaling law is valid:

$$G'(\omega) = G''(\omega) \sim \omega^{n} \quad 0<n<1 \qquad (1)$$

where n is the relaxation exponent which can give the indication about the material structure. As can be seen from the representation of the variation of the exponents n' and n'' (obtained by fitting the frequency dependence data of G' and G'' in the frequency range of 10-100 $rad \cdot s^{-1}$) with the crosslinker content, the NH_2/CHO ratio corresponding to the sol-gel transition was established at about 4.2 (n = 0.54) (Figure 4b).

The relaxation exponent, n, allows the determination of the fractal dimension, d_f, a parameter in a three-dimension space, using the relation proposed by Muthukumar [Muthukumar, 1989].

$$d_f=(10n-15)/(2n-6) \qquad (2)$$

The value of the fractal dimension (calculated with n') progressively increased from 2.05 (C3.5) to 2.44 (C1), as the citral content increased (the inset in Figure 4b, Table S1), with a d_f value of 1.95 at the gel point (NH_2/CHO = 4.2). Generally, the values of d_f are comprised between 1 and 3, the higher ones corresponding to a more compact network structure [Chambon, & Winter, 1987]. In this light, the variation of the d_f agrees well with the degree of crosslinking of the hydrogels, indicating a denser structure for the lamellar architecture (**C1**) in comparison to chitosan cross-linked by supramolecular entities (**C2-C3.5**).

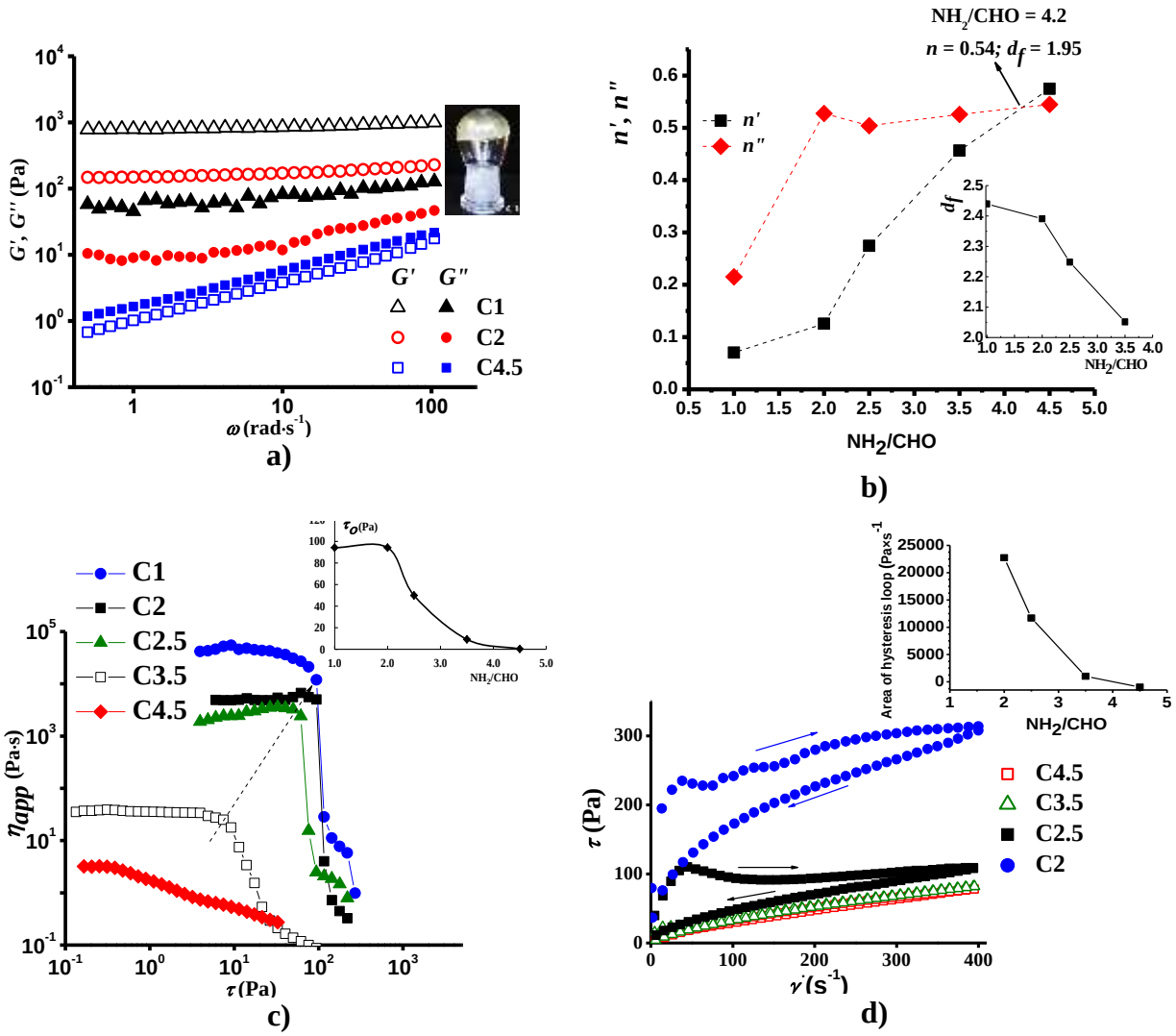

Figure 4. a) Viscoelastic moduli, *G'* and *G"* as a function of the oscillation frequency, ω, at 20 °C, for representative hydrogels; b) variation of *n'*, *n"* exponents (at 20 °C, in the frequency range of 10-100 rad·s^{-1}) as a function of NH_2/CHO ratio (the inset figure represents the dependence of the fractal dimension on NH_2/CHO ratio); c) variation of η_{app} as a function of τ for all investigated samples at 20 °C (the inset figure represents dependence of τ_o on the NH_2/CHO ratio); d) flow curves of representative hydrogels at 20 °C (the inset figure represents variation of hysteresis loop area with NH_2/CHO ratio)

Other parameters which bring information related to the viscoelastic properties of the hydrogels are the yield stress (τ_o) and zero shear viscosity (η_o). The yield stress of the samples was determined as the value at which the apparent viscosity (η_{app}) abruptly decreased as a function of shear stress (as shear stress (τ) was progressively increased) (Figure 4c).

The **C1-C3.5** hydrogel samples have shown a pseudoplastic behavior (shear-thinning behavior) with yield stress, while the **C4.5** sample did not reveal any yield stress. The hydrogels prepared with high amounts of citral (**C1**, **C2**) have shown the highest τ_o values (around 90 Pa) pointing to the formation of stiff and strong networks (in agreement with the X-ray measurements), while those with low citral content (**C3.5**) displayed a significant decline of τ_o to 9 Pa (of about tenfold) indicating a softer hydrogel with easier spreadability (inset of the Figure 4c).

Zero shear viscosity (η_o) values of the samples **C1-C4.5** as determined by applying the simplified Carreau equation to data from flow curve (the dependence of η_{app} on the shear rate ($\dot{\gamma}$)) (Table S1) [Carreau, 1972] also drastically increased as the content of citral increased, from 3.5 Pa·s for **C4.5** sample to 46 880 Pa·s for **C1** sample. The drastic increment of four orders of magnitude of the η_o is in agreement with the longer range layering (see X-ray data), revealing a close correlation between the supramolecular architecture and the hydrogel stability under the continuous shear stress of the hydrogels. Specifically, zero shear viscosity (η_o) of the **C1** hydrogel with layered architecture is about one-two orders of magnitude higher compared to the other hydrogels cross-linked by supramolecular entities (Table S1).

The oscillatory shear measurements at two different temperatures: 20 °C and 37 °C, evidenced a clear effect of the temperature on the viscoelastic parameters, especially in the case of the hydrogels crosslinked with a small quantity of citral. The elastic modulus (G') and the complex viscosity (η^*) of the investigated samples increased with the temperature (except **C2**) (Table S1). The **C2.5** and **C3.5** hydrogels undergo significant increasing of η^* at 37 °C indicating a stronger hydrogel network at the body temperature (Figure S5). This behavior is in agreement with the shift of the reaction equilibrium to the imine at higher temperature [Tang et al., 2007] and subsequent intensification of the hydrophobic interactions.

Thixotropic behavior of the samples was investigated by following the hysteresis loop formed by the flow curve at the increasing the shear rate up to 400 s^{-1} followed by its decreasing (Figure 4d). The magnitude of the hysteresis loop gives the indication on the degree of time dependency and the hysteresis area represents the energy *per* time and volume consumed in the structure breakdown. The hysteresis area is accepted to be positive for the systems with thixotropic behavior and negative if the behavior is rheopexic.

The hydrogels exhibited the upward curve above the downward curve - indicating a thixotropic behavior, while the liquid like sample **C4.5** showed the upward curve below the

downward curve – indicating a rheotropic behavior (Figure 4d). The upward curves of **C2** and **C2.5** samples present a stress overshoot (with a maximum value at about 40 s^{-1}) which can be explained by the necessity of applying a higher stress to break their strong structure and to start the flow. The sample **C3.5** with smaller content of citral showed a low area of hysteresis loop indicating that lower stress is necessary to break its weak structure. Thereby, **C2** and **C2.5** hydrogels show a strong thixotropy and **C3.5** a weak one.

The inset of figure 4d presents the dependence of the area of hysteresis loop on the crosslinker content. The hysteresis areas for **C2** and **C2.5** samples were 22 740 $Pa \cdot s^{-1}$ and 11 690 $Pa \cdot s^{-1}$, respectively, corresponding to stable structures that requires a higher energy for the structural regeneration. The investigated samples (except **C4.5**) showed a beginning of the hysteresis cycle higher than the final of the cycle, meaning that the initial apparent viscosity is higher than the final one. The percentage of the regeneration of viscosity (η_{reg}), calculated considering the viscosity value at the end of the test and the initial viscosity as reference, was found to be about 20% for **C2-C3.5** samples (Table S1).

3.6. Swelling behavior

Swelling behavior of the hydrogel samples was investigated in phosphate buffer solution (PBS) with a pH of 7.4, close to that of biological tissues and acetate buffer solution with a pH of 4, close to the one of stomach. Water was used for water uptake calculation. The mass equilibrium swelling (MES) was reached in three hours in acetate buffer, while in water and PBS it was slower, attaining the MES in 24 hours. For all the 3 media of different pH, the MES increased as the content of citral and consequently of hydrophobic associations decreased almost three fold in the case of acetate buffer solution (Figure 5). Remarkably, the xerogel samples had the MES values of about 5 times lower in PBS compared to neutral water, mostly attributed to the greater stability of the imine units in a basic solution, which suggested better preservation of the supramolecular architecture of the hydrogels in tissue engineering applications. On the contrary, the MES values were about 2 times higher in acetate buffer compared to neutral water, because of the faster reversibility of the imine bond in acidic solution resulting in the diminishing of the crosslinking density. The xerogel samples dissolved completely in 5 days in acetate buffer, while in water and phosphate buffer remained unaffected over a month. There was a close correlation between the crosslinking degree of the hydrogels and their swelling ability; the hydrogels with lower crosslinking degree and thus high amount of free hydrophilic chitosan swelled about 3 times more compared to the hydrogels with higher crosslinking degree.

The measurements were performed in triplicate and no significant differences were observed between the three samples.

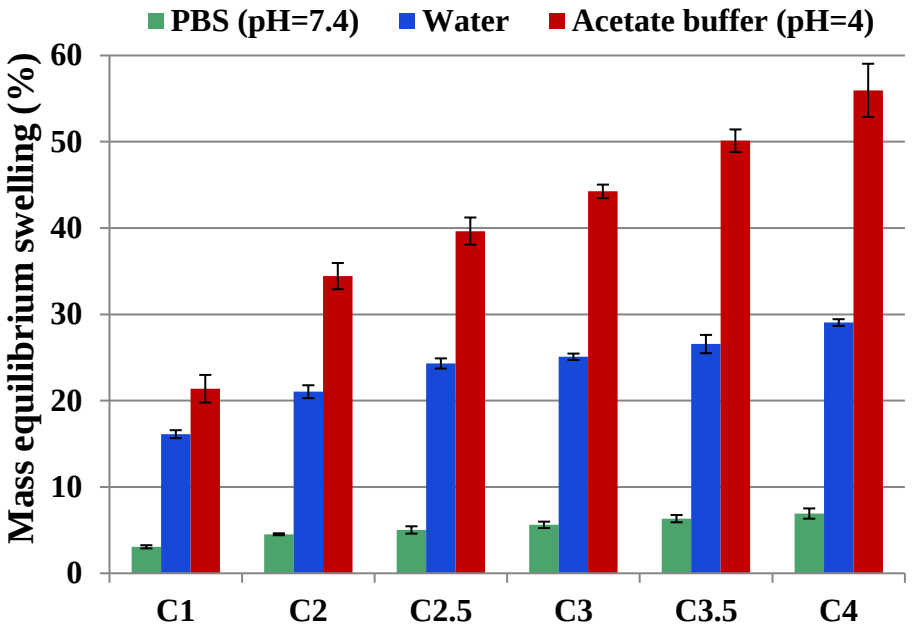

Figure 5. Mass equilibrium swelling of the hydrogels

3.7. Evaluation of the *in vivo* biocompatibility of the hydrogels

In order to use the synthesized hydrogels in bio-applications, their impact on the living organisms has been studied *in vivo* on mice, by intraperitoneal administration and determination of the hematological, biochemical and immune system profile.

The haematological tests revealed no significant changes in the number of erythrocytes, in the hemoglobin and hematocrit values, between the animals treated with **C1**, **C2**, and **C3** hydrogels compared to the animals from the control group (**C**), after 24 hours and, also, after 14 days of the experiment (Figure 6a). The values of the leukocyte formula elements - polymorphonuclear neutrophils, lymphocytes, eosinophils, monocytes, basophils - in the blood collected from the animals that received **C1**, **C2**, and **C3** respectively, were at comparable levels to those of saline-treated animals (Table S2). The hematological parameters in the normal range show the absence of a systemic inflammatory reaction related to the lack of toxicity of the hydrogels.

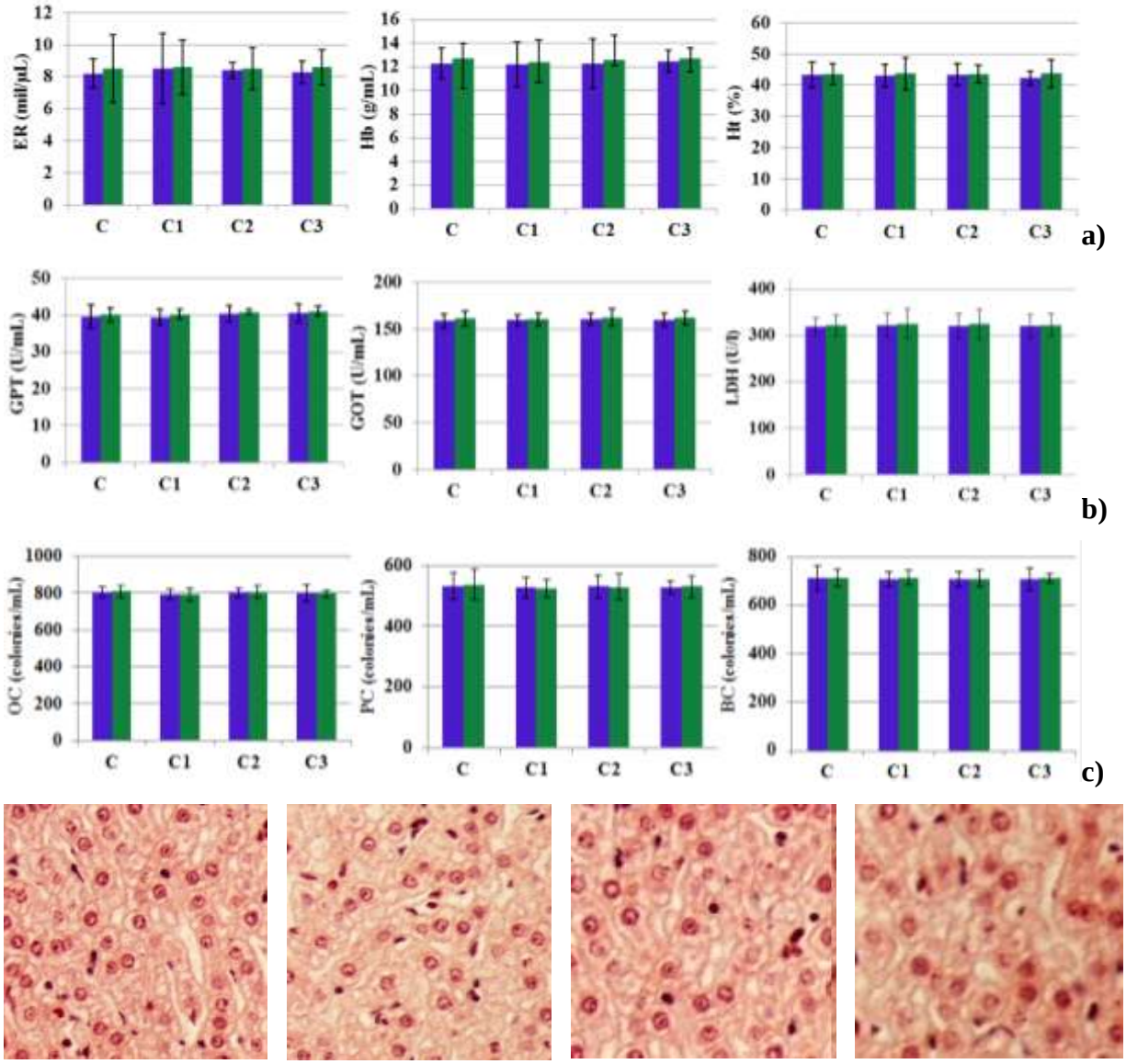

Figure 6. a) The levels of blood erythrocytes, hemoglobin and hematocrit in animals treated with **C1**, **C2**, and **C3** after one day (■) and after 14 days (■); b) The levels of GPT, GOT and LDH in animals treated with **C1**, **C2**, and **C3** and control group (**C**) after one day (■) and after 14 days (■); c) The levels of OC, PC and BC in animals treated with C1, C2, and C3 after one day (■) and after 14 days (■); The optical microscopy analysis of the liver tissue samples of d) **Control** group; e) **C1**; f) **C2**; g) **C3**; – section of liver. H&E stain x10.

Changes in the level of the alanine aminotransferase (GPT), the aspartate aminotransferase (GOT) and the lactic dehydrogenase (LDH) are commonly used as biochemical markers for liver function. As can be seen in figure 6b no statistically significant variations in the levels of GPT, GOT and LDH were noticed in the animals treated with **C1**,

C2, and **C3** hydrogels compared with the control animals, indicating a normal liver function with no observable toxicity of the studied hydrogels. Moreover, the histopathological examination of the samples prepared from liver tissue fragments of the control group animals (Figure 6d) and from animals treated with **C1**, **C2**, and **C3** respectively (Figure 6e,f,g), did not reveal any obvious changes of the normal liver architecture.

The results of immunological tests are illustrated in figure 6c. Again, as can be clearly seen from the graphs, the levels of the determined immune parameters (serum opsonic, phagocytic and bactericidal capacities) corresponding to the animals treated with **C1**, **C2**, and **C3** hydrogels, almost match the values of the control and are strongly supported by similar statistically insignificant variations. This means that the understudy hydrogels are not perceived by the immune system as dangerous or even non-self and consequently they do not stimulate an immune response in the body.

In conclusion, the synthesized citral-chitosan hydrogels did not induced any significant haematological, biochemical, immunological and histological modifications in the laboratory animals, proving *in vivo* biocompatibility under the experimental conditions.

CONCLUSIONS

Hydrogels based on chitosan and citral – two reagents from natural sources, were successfully prepared and characterized. Following the results of structural analysis, the driving force which guided the unprecedented gelling of chitosan with citral monoaldehyde was established to consist in the forming of glycodynamers by grafting dynamic imine units onto the static chitosan backbones assisted by their self-ordering through supramolecular interactions in layered architectures with role of chitosan multibinders. The ordering process was favored by the reversible nature of the imine linkages, by imination and transimination reactions which took place under the pressure of reaching a hierarchical structure of higher stability. The resulted network consisting in chitosan chains linked by the newly formed multibinders, determines robust mechanical properties, comparable with those obtained when using multi-branched crosslinkers or those appropriate to hydrogels with layered morphology given by using metallic nanosheets. The gelling process took place for low amounts of citral, starting to a 4.2/1 molar ratio of amino/aldehyde functional groups. The hydrogels were highly elastic and they showed thermo-responsiveness and thixotropic behavior. They had a sponge-like microstructure and swelled well in water and acidic solution but retained their shape in PBS solution at tissue pH. Their morphology could be tuned by the crosslinking degree.

As expected, the evaluation of the i*n vivo* biocompatibility of the hydrogels, monitored on laboratory mice, did not result in any abnormal changes in the hematological, biochemical and immune system profile, recommending their safe use in bio-applications.

The paper brings into attention a novel hydrogel with real chances for bio-applications. Moreover, it illustrates a novel method of crosslinking chitosan using monoaldehydes which are abundant in nature and have own valuable therapeutic properties.

ACKNOWLEDGEMENTS

The research leading to these results has received funding from the Romanian National Authority for Scientific Research, MEN – UEFISCDI grant, project number PN-II-RU-TE-2014-4-2314. This publication is part of a project that has received funding from the European Union's Horizon 2020 research and innovation programme under grant agreement 667387.

REFERENCES

Ailincai, D., Marin, L., Morariu, S., Mares, M., Bostanaru, A.C., Pinteala, M., Simionescu, B.C. & Barboiu, M. (2016). Dual crosslinked iminoboronate-chitosan hydrogels with strong antifungal activity against Candida planktonic yeasts and biofilms. *Carbohydrate Polymers*, *152*, 306-316.

Amar-Iuli, I., & Garti, N. (2006). Progress in Structural Transformation in Lyotropic Liquid Crystals in *Colloid Stability*, Weinheim: Willey-VCH.

Baron, M. (2001). Definitions of Basic Terms Relating to Low-Nolar-Mass and Polymer Liquid Crystals. *Pure and Applied Chemistry*, *73*, 845-895.

Beauchamp, R.O., St Clair, M.B., Fennell, T.R., Clarke, D.O., & Morgan, K.T. (1992). A Critical Review of the Toxicology of Glutaraldehyde. *Critical Reviews in Toxicology 22*, 143-174.

Berger, J., Reist, M., Mayer, J.M., Felt, O., Peppas, N.A., & Gurny, R. (2004). Structure and Interactions in Covalently and Ionically Crosslinked Chitosan Hydrogels for Biomedical Applications. *European Journal of Pharmaceutics and Biopharmaceutics*, *57*, 19-34.

Beskardes, I.G., Demirtas, T.T., Durukan, M.D., & Gumusderelioglu, M. (2015). Microwave Assisted Fabrication of Chitosan Hydroxyapatite Superporous Hydrogel Composites as Bone Scaffolds. *Journal of Tissue Engoneering and Regenerative Medicine*, *9*, 1233-1246.

Carreau, P.J. (1972). Rheological Equations from Molecular Network Theories. *Journal of Rheology*, *16*, 99-127.

Chambon, F., & Winter, H.H. (1987). Linear Viscoelasticity at the Gel Point of a Crosslinking PDMS with Imbalanced Stoichiometry, *Journal of Rheology*, *31*, 683-697.

Chang, R., Wang, X., Li, X., An, H., & Qin, J. (2016). Self-Activated Healable Hydrogels with Reversible Temperature Responsiveness. *ACS Applied Materials & Interfaces*, 8, 25544-25551.

Chawla, P., Srivastava, R., Pandey, P., & Chawla V. (2014). Hydrogels: A Journey from Diapers to Gene Delivery. *Mini Reviews in Medicinal Chemistry*, *14*, 154-167.

Chen, H., Hu, X., Chen, E., Wu, S., McClements, D.J., Kiu, S., Li, B., & Li, Y. (2016). Preparation, Characterization, and Properties of Chitosan Films with Cinnamaldehyde Nanoemulsions. *Food Hydrocolloid*, *61*, 662-671.

Chen, L., Chen, Z., Li, X., Huang, W., Li, X., & Liu, X. (2013). Dynamic Imine Chemistry Assisted Reaction Induced Hetero-Epitaxial Crystallization: Novel Approach towards Aromatic Polymer/CNT Nanohybrid Shish-Kebabs and Related Hybrid Crystalline Structures, *Polymer*, *54*, 1739-1745.

Chen, Z., Jiang, Y., Chen, L., Huang, W., Li, X., Li, X., & Liu, X. (2013). Solvothermal Synthesis of Polyazomethine Microspheres by Pickering Emulsion Templates and their Transformation into Complex Microtubes and Anisotropic Hollow Spheres Enabled by Dynamic Imine Chemistry. *Polymer Journal*, 45, 1087-1093.

Clima, L., Peptanariu D., Pinteala M., Salic, A., & Barboiu, M. (2015). Dynavectors: Dynamic Constitutional Vectors for Adaptive DNA Transfection. *Chemical Communication*, *51*, 17529-17531.

Dabrowski, R. (2015). From the Discovery of the Partially bilayer Smectic a Phase to Blue Phases in Polar Liquid Crystals. *Liquid Crystals*, *42*, 783-818.

De Jong, W.H., Carraway, J.W., & Geertsma, R.E. (2012) In vivo and in vitro testing for the biological safety evaluation of biomaterials and medical devices, *in Biocompatibility and Performance of Medical Devices*, Woodhead Publishing, 120-158.

Desbrires, J., Martinez, C., & Rinaudo, M. (1996). Hydrophobic Derivatives of Chitosan: Characterization and Rheological Behavior. *International Journal of Biological Macromolecules*, *19*, 21-28.

Destri, S., Khotina, I.A., & Porzio, W. (1998). 3-Hexyl Tetra-Substituted Sesquithienylene-Phenylene Polyazomethines with High Molecular Weight. Mechanistic Considerations. *Macromolecules*, 31, 1079-1086.

Dinu M.V., Ozmen, M.M., Dragan, E.Z., & Okay, O. (2007). Freezing as a Path to Build Macroporous Structures: Superfast Responsive Polyacrylamide Hydrogels. *Polymer*, *48*, 195-204.

Garnicia-Palafox, I.M., & Sanchez-Arevalo, F.M. (2016). Influence of Natural and Synthetic Crosslinking Reagents on the Structural and Mechanical Properties of Chitosan-based Hybrid Hydrogels. *Carbohydrate Polymers*, *151*, 1073-1081.

Hu, L., Zhang, Y., & Ramström, O. (2015). Gelation-driven Dynamic Systemic Resolution: *in situ* Generation and Self-Selection of an Organogelator, *Scientific Reports 5*, 11065-11071.

Huber, D., Tegl, G., Baumann, M., Sommer, E., Gorji, E. G., Borth, N., Schleining, G., Nyanhongo, G. S. Guebitz, G. M. (2017). Chitosan hydrogel formation using laccase activated phenolics as cross-linkers. *Carbohydrate Polymers*, *157*, 814-822.

Iftime, M., Morariu, S., & Marin, L. (2017). Salicyl-imine-chitosan hydrogels. Supramolecular architecturing as a crosslinking method toward multifunctional hydrogels. *Carbohydrate Polymers*, *265*, 39-50.

Jayakumar, R. Menon, D., Manzoor, K., Nair, S. V., & Tamura, H. (2010). Biomedical applications of chitin and chitosan based nanomaterials – a short review, *Carbohydrate Polymers*, 82, 227-232.

Jayakumar, R., Chennazhi, K. P., Muzzarelli, R. A. A., Tamura, H., Nair, S. V., & Selvamurugan, N. (2010). Chitosan conjugated DNA nanoparticles in gene therapy, *Carbohydrate Polymers*, 79, 1-8.

Jing, G., Wang, L., Yu, H., Amer, A. W., & Zhang, L. (2013). Recent Progress on Study of Hybrid Hydrogels for Water Treatment. *Colloids and Surfaces A*, *416*, 86-94.

Kamata, H., Li, X., Chung, U., & Sakai, T. (2015). Design of Hydrogels for Biomedical Applications. *Advanced Healthcare Materials*, *4*, 2360-2374.

Kaya, I., & Kilavuz, E. (2015). Novel Multicolor Schiff Base Polymers Prepared via Oxidative Polycondensation, *Journal of Fluorescence*, *25*, 663-673.

Kumirska, J., Czerwicka, M., Kaczyński, Z., Bychowska, A., Brzozowski, K., Thöming, J., & Stepnowski, P. (2010). Application of Spectroscopic Methods for Structural Analysis of Chitin and Chitosan. *Marine Drugs*, *8*, 1567-1636.

Leceta, I., Guerrero, P., Ibarburu, I., Dueñas, M. T., & de la Caba, K. (2013). Characterization and Antimicrobial Analysis of Chitosan-based Films. *Journal of Food Engineering*, *116*, 889-899.

Limon-Pacheco, J., & Gonsebatt, M.E. (2009). The Role of Antioxidants and Antioxidant Related Enzymes in Protective Responses to Environmentally Induced Oxidative Stress. *Mutation Research/Genetic Toxicology and Environmental Mutagenesis*, 674, 137-147.

Liu, M., Ishida, Y., Ebina, Y., Sasaki, T., & Aida, T. (2013). Photolatently modulable hydrogels using unilamellar titania nanosheets as photocatalytic crosslinkers. *Nature*, *4*, art no. 2029.

Liu, Y., & Li Z.T. (2013). A Dynamic Route to Structure and Function: Recent Advances in Imine-Based Organic Nanostructured Materials. *Australian Journal of Chemistry*, *66*, 9-2.

Liu, Y., Lehn, J-M., & Hirsch, A.K.H. (2016). Molecular Biodynamers: Dynamic Covalent Analogues of Biopolymers. Accounts of Chemical Research, 10.1021/acs.accounts.6b00594

Marin, L., Ailincai, D., Calin, M., Stan, D., Constantinescu, C.A., Ursu, L., Doroftei, F., Pinteala, M., Simionescu, B.C., & Barboiu, M. (2016). Dynameric Frameworks for DNA Transfection, *ACS Biomaterials Science & Engineering*, *2*, 104-111.

Marin, L., Ailincai, D., Mares, M., Paslaru, E., Cristea, M., Nica, V., & Simionescu, B.C. (2015). Imino-Chitosan Biopolymeric Films. Obtaining, Self-assembling, Surface and Antimicrobial Properties. *Carbohydrate Polymyrs*, *117*, 762-770.

Marin, L., Destri, S., Porzio, W., & Bertini, F. (2009). Synthesis and characterization of new azomethine derivatives exhibiting liquid crystalline properties. *Liquid Crystals*, *36*, 21-32.

Marin, L., Morariu, S., Popescu, M.-C., Nicolescu, A., Zgardan, C., Simionescu, B.C., & Barboiu, M. (2014). Out-of-Water Constitutional Self-Organization of Chitosan–Cinnamaldehyde Dynagels. *Chemistry Europeean Journal*, *20*, 4814-4821.

Marin, L., Simionescu, B.C., & Barboiu M. (2012). Imino-chitosan biodynamers. *Chemical Communications*, *48*, 8778-8780.

Marin, L., van der Lee, A., Shova, S., Arvinte, A. & Barboiu, M. (2015). Molecular amorphous glasses toward large azomethine crystals with aggregation-induced emission. *New Journal of Chemistry*, *39*, 6404-6420.

Mikhailov, S.N., Zakharova, A.N., Drenichev, M.S., Ershov, A.V., Kasatkina, M.A., Vladimirov, L.V., Novikov, V.V., & Kildeeva, N.R. (2016). Crosslinking of Chitosan with Dialdehyde Derivatives of Nucleosides and Nucleotides. Mechanism and Comparison with Glutaraldehyde. *Nucleosides Nucleotides and Nucleic Acids*, *35*, 114-129.

Morariu, S., Bercea, M., & Brunchi, C.-E. (2015). Effect of Cryogenic Treatment on the Rheological Properties of Chitosan/Poly(Vinyl Alcohol) Hydrogels. *Industrial & Engineering Chemical Research*, *54*, 11475-11482.

Muthukumar, M. (1989). Screening Effect on Viscoelasticity near the Gel Point. *Macromolecules*, *22*, 4656-4658.

Padmanabhan, A. & Nair, L.S. (2016). *Chitin and Chitosan for Regenerative Medicine* India: Springer, P.K. Dutta (ed.).

Rinaudo, M. (2006). Chitin and chitosan: Properties and Applications. *Progress in Polymer Science*, 31, 603-632.

Roy, N., Bruchmannb, B., & Lehn, J.M. (2015). Dynamers: Dynamic Polymers as Self-Healing Materials. *Chemical Society Reviews 44*, 3786-3807.

Safoura, F. (2014). Novel Synthesis of Schiff bases Bearing Glucosamine. *Research Journal of Chemical Sciences*, 4, 25-28.

Schneider, M.W., Siegfried Hauswald H.J., Stoll, R., & Mastalerz, M. (2012). A Shape Persistent Exo-Functionalized [4 + 6] Imine Cage Compound with a Very High Specific Surface Area. *Chemical Communication, 48,* 9861-9863.

Sek, D., Grucela-Zajac, M., Krompiec, M., Janeczek, H., & Schab-Balcerzak, E. (2012). New Glass Forming Triarylamine based Azomethines as a Hole Transport Materials: Thermal, Optical and Electrochemical Properties. *Optical Materials*, 34, 1333-1346.

Sek, D., Jarzabek, B., Grabiec, E., Kazmarczyk, B., Janeczek, H., Sikora, A., Hreniak, A., Palewicz, M., Lapkowski, M., Karon, K., & Iwan, A. (2012) A Study of Thermal, Optical and Electrical Properties of New Branched Triphenylamine Based Polyazometines. *Synthetic Metals*, *160*, 2065-2076.

Sharma, R., Bajpai, J., Bajpai, A.K., Acharya, S., Shrivastaya, R.B., & Shukla, S.K. (2014). Designing Slow Water Releasing Alginate Nanoreserviors for Sustained Irrigation in Scanty Rainfall Areas. *Carbohydrate Polymers*, *102*, 513-520.

SIDS Initial Assessment for 13th SIAM, Citral CAS No. 5392-40-5, 2001.

Sreenivasachary N. & Lehn, J.M. (2005). Gelation-Driven Component Selection in the Generation of Constitutional Dynamic Hydrogels Based on Guanine-Quartet Formation. *Proceedings of the National Academy of Sciences*, *102*, 5938-5943.

Suryanaraya, C., & Grant, M.N. (1998). *X-ray Diffraction: a Practical Approach*, New York: Springer Science.

Tang, Y.F., Du, Y.M., Hu, X.W., Shi, X.W., & Kennedy, J.F. (2007). Rheological characterisation of a novel thermosensitive chitosan/poly(vinyl alcohol) blend hydrogel. *Carbohydrate Polymers*, 67, 491-499.

vu Deb Linde, R., Dornseiffen, J. W., Veenland, J. U., & de Boer, T. J. (2016). Proton magnetic resonance spectra of some methyl substituted N-methylbensophenonimines and benzophenonimines. *Spectrochimica Acta*, 351, 375-334.

Wang, Q., Mynar, J.L., Yoshida, M., Lee, E., Okura, K., Kinbara, K., & Aida, T. (2010). High Water Content Mouldable Hydrogels by Mixing Clay and a Dendritic Molecular Binder, *Nature*, *463*, 339-343.

Wolf, M.F., & Andwraon, J.M. (2012). Practical approach to blood compatibility assessments: general considerations and standards, *in Biocompatibility and Performance of Medical Devices*, Woodhead Publishing, 159-200, 201-206.

Zabulica, A., Balan, M., Belei, D., Sava, M., Simionescu B.C., & Marin, L. (2013). Novel Luminescent Phenothiazine based Schiff Bases with Tuned Morphology. Synthesis, Structure, Photophysical and Thermotropic Characterization. *Dyes and Pigments*, *96*, 686-698.

Zabulica, A., Perju, E., Bruma, M., & Marin, L. (2014). Novel luminescent liquid crystalline polyazomethines. Synthesis and study of thermotropic and photoluminescent properties. *Liquid Crystals*, *41*, 252-262.

Zaltariov, M.F., Cazacu, M., Racles, C., Musteata, V., Vlad, A., & Airinei, A. (2015). Metallopolymers Based on a Polyazomethine Ligand Containing Rigid Oxadiazole and Flexible Tetramethyldisiloxane Units. *Journal of Applied Polymer Science*, *132*, 41631-41642.

Zhang, Y., & Barboiu, M. (2016). Constitutional Dynamic Materials—Toward Natural Selection of Function. *Chemical Reviews*, *116*, 809-834.

TOC graphic